AIAA JOURNAL
Vol. 39, No. 3, March 2001

Simulating the Nonlinear Dynamics of an Elastic Cable

Jeffrey W. Yokota* and Seifu A. Bekele†
University of Alberta, Edmonton, Alberta T6G 2G8, Canada
and
David J. Steigmann‡
University of California, Berkeley, Berkeley, California 94720-1740

We present a new technique for simulating the time-dependent behavior of an elastic material in general and the nonlinear dynamics of a linearly elastic cable in particular. Results will be presented for both the small displacement of a highly nonlinearly elastic material and the large displacement of a linearly elastic cable. The first simulation, a small displacement of a nonlinearly elastic material, will be used to validate our numerical scheme against a known analytical solution while the second simulation, the large displacement of a linearly elastic cable, will be used to investigate the looping that can occur when wave interactions produce regions of strong local compression.

I. Introduction

THE nonlinear dynamics of an elastic cable are extremely important to such phenomena as the towing of marine vehicles and the deployment of tethered payloads in space. As a payload is deployed, it oscillates between free flight and impact, thus producing a dangerous loading and unloading that can leave the tether vulnerable to knotting.[1] Unfortunately most investigations are of either a postdeployment configuration, a tether in tension that is never unloaded,[2] or a benign deployment where the cable is unloaded but undergoes only a small displacement.[3]

Analytical results have been obtained for both loaded[4] and unloaded[5] cables, but it is required that transverse oscillations be significantly less than the longitudinal waves and that no wave reflections be present in the elastic media. Investigations have also shown that significant linear tension waves can be produced by purely transverse initial deflections, provided a cable's unloaded equilibrium configuration is one in tension.[6] However, although analytical investigations have produced significant insight into the understanding of wave propagation they are not capable of predicting the highly nonlinear wave interactions that are responsible for knotting an elastic cable.

Thus, we present a numerical technique for simulating the time-dependent behavior of an elastic material in general and the nonlinear dynamics of a linearly elastic cable in particular. Our scheme solves the system of second-order partial differential equations, which describes the force balance across an elemental segment of a flexible cable. These equations are approximated by a third-order-accurate, fully implicit time integration whose spatial terms are constructed from a second-order-accurate force balance across each of the finite mesh cells. By solving these equations in their second-order form, we can simulate the nonlinear dynamics of an elastic material without having to account for the loss of hyperbolicity that is likely to occur within its first-order counterpart.[7]

Nonlinear motions can be produced by either a small displacement of a highly nonlinearly elastic material or a large displacement of a linearly elastic media. In the work to follow, we will present simulations of both these situations. The first simulation, a small displacement of a nonlinearly elastic material, will be used to validate our numerical scheme against a known analytical result,[8] whereas our second simulation, the large displacement of a linearly elastic cable, will be used to investigate the looping of a visco-elastic cable. This highly nonlinear motion, generated by the large displacement of the elastic material, is initiated by an impact pressure loading and unloading of a visco-elastic cable. This construction, although arguably more academic than practical, was chosen to avoid the shock-capturing/shock-fitting requirements of a nonlinearly elastic material.[9] A shock treatment based on anything more sophisticated than simple esthetics would have to be constructed from a first-order hyperbolic form of the the governing equations and the method of characteristics. Unfortunately our results show that the looping of an elastic cable appears to be related to the presence of local compression, the very condition that renders the method of characteristics invalid.[7] Thus, our numerical scheme is first validated against the analytical description of a small displacement unloading of a nonlinearly elastic material and then used to simulate the looping that can be caused by the large displacement unloading of a linearly elastic cable.

II. Governing Equations

Given both an external force $\boldsymbol{b}$ and a net external pressure p, acting on the elemental line segment ∂s of a flexible cable, we can write, for all time t, the following force balance[10]:

$$(\boldsymbol{f}_R - \boldsymbol{f}_L) - p\wp\partial s\boldsymbol{n} + \boldsymbol{b} = \partial m\frac{\partial^2\boldsymbol{r}}{\partial t^2} \tag{1}$$

where $\boldsymbol{f}_R$ and $\boldsymbol{f}_L$ are the internal resistance forces generated on the right and left ends of the segment's deformed configuration while $\wp$, ∂m, $\boldsymbol{r}$, and $\boldsymbol{n}$ are its cross-sectional perimeter, mass, local position vector, and outward surface normal, respectively. The conservation of mass allows us to write

$$\partial m = \rho a\partial s = \rho A\partial S \tag{2}$$

where ρ is density; a is the cross-sectional area of the segments deformed configuration; and A and ∂S are the cross-sectional area and arc length of the segment's initial, undeformed configuration, respectively. Thus, we can construct the following equation of motion:

$$\frac{\partial\boldsymbol{f}}{\partial S} - p\wp\frac{\partial s}{\partial S}\boldsymbol{n} + \frac{\boldsymbol{b}}{\partial S} = \rho A\frac{\partial^2\boldsymbol{r}}{\partial t^2} \tag{3}$$

which, given that local stretch is defined as

$$\lambda = \frac{\partial s}{\partial S} = \sqrt{\frac{\partial r_i}{\partial S}\frac{\partial r_i}{\partial S}} \tag{4}$$

can be written as

$$\frac{\partial\boldsymbol{f}}{\partial S} - p\wp\lambda\boldsymbol{n} + \frac{\boldsymbol{b}}{\partial S} = \rho A\frac{\partial^2\boldsymbol{r}}{\partial t^2} \tag{5}$$

Here we can say that the cable is being elongated when $\lambda > 1$ and compressed when $\lambda < 1$. We can also define the local strain as

$$\delta = \lambda - 1 \tag{6}$$

Received 7 August 2000; revision received 12 September 2000; accepted for publication 20 September 2000. Copyright © 2000 by the American Institute of Aeronautics and Astronautics, Inc. All rights reserved.

*Associate Professor, Department of Mechanical Engineering. Senior Member AIAA.
†Research Assistant, Department of Mechanical Engineering.
‡Associate Professor, Department of Mechanical Engineering.

and note that the condition $\lambda \geq 1$ minimizes the potential energy of an equilibrium configuration and need occur only at steady state.[11] Thus, during an unsteady simulation, we would not be surprised to find the local stretch dipping below unity and fully expect it to do so during large-amplitude, nonlinear motions that are far from its equilibrium configuration. In fact, Dickey[12] has shown that compressive solutions can exist whenever an unloaded cable's vertical displacements are nonmonotonic and, under certain circumstances, even when lightly loaded.

We can define an internal force as

$$\boldsymbol{f} = \sigma a \boldsymbol{l} \tag{7}$$

where σ is the local stress and $\boldsymbol{l}$ is the unit tangent vector. Given that

$$l_i = \frac{\partial r_i}{\partial s} = \frac{\partial r_i}{\partial S}\frac{1}{\lambda} \tag{8}$$

and assuming Hooke's law, a linear relationship between stress and strain

$$\sigma a = EA(\lambda - 1) \tag{9}$$

where E is Young's elastic modulus, we can then rewrite the internal force as

$$f_i = EA\left(1 - \frac{1}{\lambda}\right)\frac{\partial r_i}{\partial S} \tag{10}$$

which allows us to write our equation of motion, Eq. (5), as

$$\frac{\partial}{\partial S}\left[EA\left(1 - \frac{1}{\lambda}\right)\frac{\partial r_i}{\partial S}\right] - p_{\wp}\lambda n_i + \frac{b_i}{\partial S} = \rho A \frac{\partial^2 r_i}{\partial t^2} \tag{11}$$

A. Visco-Elastic Equations

To avoid the numerical dispersion errors that are often generated near sharp gradients and ensure that our simulations converge to a steady equilibrium configuration, we have added a dissipation model to the equations, Eqs. (11), that would otherwise be perfectly elastic. Nonlinear solutions often contain sharp spatial gradients that are not easily reproduced numerically. Thus, artificial dissipation models are often added to suppress the numerical Gibbs phenomena that can occur near sharp gradients. Internal friction forces are modeled by a linear Voigt visco-elastic term[13,14] of the form

$$f_{v_i} = \mu A \frac{\partial^2 \boldsymbol{r}}{\partial S \partial t} \tag{12}$$

where μ is the material's extensional viscosity and the resulting equations of motion can be written

$$\frac{\partial}{\partial S}\left[EA\left(1 - \frac{1}{\lambda}\right)\frac{\partial r_i}{\partial S} + \mu A \frac{\partial^2 \boldsymbol{r}}{\partial S \partial t}\right] - p_{\wp}\lambda n_i + \frac{b_i}{\partial S} = \rho A \frac{\partial^2 r_i}{\partial t^2} \tag{13}$$

B. Two-Dimensional Equations

To avoid the difficulties of modeling impact and rebound forces, we have assumed that the cable can fold past, but not back onto itself. When this phenomenon begins to occur, the cable is allowed to fold past itself, creating loops or knots instead of colliding and rebounding, elastically or otherwise. Thus, without a loss of generality, we can describe the motion of this cable in an essentially two-dimensional plane. Although this two-dimensional approximation is arguably more academic than practical, one can easily imagine this two-dimensional looping process as being the first step in the more complicated three-dimensional knotting phenomena. In two dimensions the unit normal can be defined as

$$\lambda n_i = \lambda(\boldsymbol{k} \times \boldsymbol{l}) = \epsilon_{ij}\frac{\partial r_j}{\partial S} \tag{14}$$

where ϵ_{ij} is the alternating tensor with components $\epsilon_{11} = \epsilon_{22} = 0$, $\epsilon_{12} = 1$ and $\epsilon_{21} = -1$. Thus, Eq. (13) becomes the following nonlinear, coupled system:

$$\frac{\partial}{\partial S}\left[EA\left(1 - \frac{1}{\lambda}\right)\frac{\partial r_1}{\partial S} + \mu A \frac{\partial^2 r_1}{\partial S \partial t}\right] - p_{\wp}\frac{\partial r_2}{\partial S} = \rho A \frac{\partial^2 r_1}{\partial t^2} \tag{15}$$

$$\frac{\partial}{\partial S}\left[EA\left(1 - \frac{1}{\lambda}\right)\frac{\partial r_2}{\partial S} + \mu A \frac{\partial^2 r_2}{\partial S \partial t}\right] + p_{\wp}\frac{\partial r_1}{\partial S} = \rho A \frac{\partial^2 r_2}{\partial t^2} \tag{16}$$

which we can solve in the nondimensional form

$$\frac{\partial^2 \boldsymbol{W}}{\partial t^2} = \frac{\partial \boldsymbol{F}}{\partial S} + \boldsymbol{B} \tag{17}$$

where

$$\boldsymbol{W} = \begin{bmatrix} r_1 \\ r_2 \end{bmatrix}, \qquad \boldsymbol{F} = \begin{bmatrix} \left(1 - \frac{1}{\lambda}\right)\frac{\partial r_1}{\partial S} + \tilde{\mu}\frac{\partial^2 r_1}{\partial S \partial t} \\ \left(1 - \frac{1}{\lambda}\right)\frac{\partial r_2}{\partial S} + \tilde{\mu}\frac{\partial^2 r_2}{\partial S \partial t} \end{bmatrix}$$

$$\boldsymbol{B} = \begin{bmatrix} -\tilde{P}\frac{\partial r_2}{\partial S} \\ \tilde{P}\frac{\partial r_1}{\partial S} \end{bmatrix} \tag{18}$$

and $\tilde{\mu} = (\mu/E)\sqrt{(\rho L^2/E)}$ is called the loss coefficient, $\tilde{p} = p_{\wp}L/EA$ a nondimensional pressure, and L a reference length. We note that Dickey[12] has shown that compressive solutions can only exist when a cable's vertical displacements are nonmonotonic and $(p_{\wp}L/A)^2 < E^2$. In the simulations to follow, we have employed a loss coefficient of $\tilde{\mu} = 2.5 \times 10^{-4}$, which is typical of such metals as aluminum, copper, or steel alloy. To this cable we have applied a vertical pressure loading of a magnitude and duration large enough to generate the amplitude displacements needed to produce both a nonmonotonic and compressive behavior.

III. Numerical Construction

The equations of motion just described, Eqs. (18), are integrated in time by the following higher-order accurate, fully implicit scheme[15]:

$$\frac{\eta_1 \boldsymbol{W}^{n+1} + \eta_2 \boldsymbol{W}^{n} + \eta_3 \boldsymbol{W}^{n-1} + \eta_4 \boldsymbol{W}^{n-2} + \eta_5 \boldsymbol{W}^{n-3}}{\Delta t^2} = \left[\frac{\partial \boldsymbol{F}}{\partial S} + \boldsymbol{B}\right]^{n+1} \tag{19}$$

The spatial terms in this scheme are approximated by second-order-accurate central differences, whereas the temporal terms are constructed from one-sided differences of second-order accuracy or higher. In fact, by choosing $\eta_1 = \frac{35}{12}$, $\eta_2 = -\frac{104}{12}$, $\eta_3 = \frac{114}{12}$, $\eta_4 = -\frac{56}{12}$, and $\eta_5 = \frac{11}{12}$ we can obtain an approximation to the second derivative in time that is both third-order accurate and dissipative. By ensuring that the leading terms of this approximation's truncation error are diffusive rather than a dispersive, one hopes it minimizes the likelihood of generating any numerical Gibbs phenomena near sharp gradients. In fact our studies have shown that numerical oscillations, comparable to those obtained in transonic flow simulations, can be produced by a centrally differenced, second-order-accurate approximation. Because we have chosen not to transform our governing equations into a first-order hyperbolic system, we cannot employ either of the well-known shock-capturing techniques of explicitly added artificial dissipation[16] or higher-order upwind differencing.[17] Thus, considerable effort was made to tailor our numerical scheme into a form whose truncation error was both higher-order accurate and dissipative. By choosing to solve the governing equations in their second-order form, we can simulate wave interactions that result in regions of local compression. Unlike the method of characteristics, which is based on the first-order form of the governing equations, our numerical scheme is not rendered invalid by the loss of hyperbolicity[7] that occurs when $\lambda < 1$. Furthermore, the symmetry of our spatial approximations allows us to capture physical

symmetries for durations longer than could be expected from a hyperbolic upwind scheme. In fact our results will show that the unloading of a visco-elastic cable can be simulated to its final equilibrium state without a significant loss of symmetry.

Because these equations are nonlinear, the implicit terms must be constructed with considerable care. Approximate factorization schemes[18–20] achieve considerable numerical efficiency, at the expense of a reduction in time accuracy, by linearizing the implicit terms within each time step. These schemes are suitable for steady-state simulations but less than ideal for time-accurate ones. Thus, we have chosen to follow Jameson's approach[21] and have embedded within each time step an iteration procedure that allows us to construct the implicit terms without employing an approximate factorization. This procedure can be described by first constructing the residual

$$\boldsymbol{R} = \frac{\eta_1 \boldsymbol{W}^{n+1} + \eta_2 \boldsymbol{W}^{n} + \eta_3 \boldsymbol{W}^{n-1} + \eta_4 \boldsymbol{W}^{n-2} + \eta_5 \boldsymbol{W}^{n-3}}{\Delta t^2} - \left[\frac{\partial \boldsymbol{F}}{\partial S} + \boldsymbol{B}\right]^{n+1} \tag{20}$$

and then defining a fictitious first-order ordinary partial differential equation of the form

$$\frac{\partial \boldsymbol{W}^*}{\partial t^*} + \boldsymbol{R}^* = 0 \tag{21}$$

where

$$\boldsymbol{R}^* = \eta_1 \frac{\boldsymbol{W}^*}{\Delta t^2} - \left[\frac{\partial \boldsymbol{F}}{\partial S} + \boldsymbol{B}\right]^* + \frac{\eta_2 \boldsymbol{W}^{n} + \eta_3 \boldsymbol{W}^{n-1} + \eta_4 \boldsymbol{W}^{n-2} + \eta_5 \boldsymbol{W}^{n-3}}{\Delta t^2} \tag{22}$$

and $\boldsymbol{W}^* \rightarrow \boldsymbol{W}^{n+1}$ when the fictitious time-dependent equation converges to the steady-state solution

$$\frac{\partial \boldsymbol{W}^*}{\partial t^*} = \boldsymbol{R}^* = 0 \tag{23}$$

To converge this fictitious unsteady equation, Eq. (22), to its steady state, we have chosen to integrate it with a four-stage Runga–Kutta scheme[22] whose coefficients $\alpha_1 = \frac{1}{4}$, $\alpha_2 = \frac{1}{4}$, $\alpha_3 = \frac{1}{2}$, and $\alpha_4 = 1$ are chosen to enhance steady-state convergence. In each of the simulations to follow, using a fictitious time step of size $\Delta t^* = 1.25 \times 10^{-7}$, we were able to reduce the average residual $\bar{R}^*$ to at least $\mathcal{O}(10^{-9})$ within 15 iterations.

IV. Code Validation

To validate our code against an analytical solution, we have chosen to simulate the dynamics of a transversely impacted cable. Given an elastic cable whose internal forces are governed by the nonlinear Mooney–Rivlin constitutive relation[23,24]

$$f_i = \frac{EA}{\lambda}\left[\beta - \frac{(1-\beta)}{\lambda}\left(\lambda - \frac{1}{\lambda^2}\right)\right]\frac{\partial r_i}{\partial S} \tag{24}$$

where $0 \leq \beta \leq 1$, Wegner and Haddow[8] have shown that an analytical solution can be constructed for the case in which one end of an initially horizontal cable is displaced by a constant vertical velocity while the other end is held constant. This transverse impact propagates disturbances through the cable by the following longitudinal and transverse wave speeds:

$$C_L = \pm\left\{\frac{EA}{\rho}\left[\beta\left(1 - \frac{2}{\lambda^3}\right) + \frac{3(1-\beta)}{\lambda^4}\right]\right\}^{\frac{1}{2}} \tag{25}$$

$$C_T = \pm\left\{\frac{EA}{\rho}\left[\beta + \frac{(1-\beta)}{\lambda}\right]\left(1 - \frac{1}{\lambda^3}\right)\right\}^{\frac{1}{2}} \tag{26}$$

which are both unsteady and nonlinear.

To simulate this motion, we first select $\beta = 0.6$, a value most appropriate for simple tension,[8] and then set one end of the cable in motion with a nondimensional velocity of unit value. For a cable of length $l = 1$ and a uniform grid spacing of $\Delta S = 2 \times 10^{-3}$, a time step size of $\Delta t = 5 \times 10^{-4}$, or a Courant number of $Cn = 0.25$, was chosen to time advance our calculations.

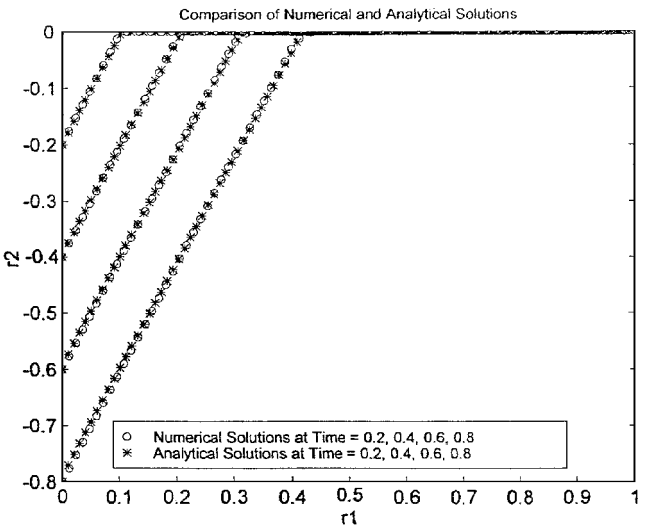

Fig. 1 String position: nonlinearly elastic cable.

Shown in Fig. 1 are the cable positions at nondimensional times of $t = 0.2, 0.4, 0.6, 0.8$. Here the left end of the string is pulled downward with a constant vertical velocity while the remainder of the string is allowed to respond accordingly. Given that a timescale of $t = 1$ is needed to traverse the end of our cable a vertical distance equal to its original length, the results shown in Fig. 1 have occurred before the longitudinal waves could reached the fixed end of the cable. From these results, after 1600 time steps we can see only a marginal difference between the numerical and analytical solutions. At each of these moments in time, the wave disturbances have been captured by our numerical scheme with an accuracy that is immediately obvious. In fact, the error in the angle between the cable's current and original positions is less than 2% and shows that the nonlinear wave speeds of Eqs. (27) and (28) have been captured accurately by our numerical scheme.

V. Pressure Impacted Cable

To investigate the nonlinear dynamics of an elastic cable, we first return to Hooke's law and its linear model of the internal restoring forces, Eq. (10). This model results in the following longitudinal and transverse wave speeds:

$$C_L = \pm(EA/\rho)^{\frac{1}{2}} \tag{27}$$

$$C_T = \pm[(EA/\rho)(1 - 1/\lambda)]^{\frac{1}{2}} \tag{28}$$

from which it becomes clear that the propagation of small disturbances will be linear because the longitudinal velocity, which it constant, will dominate over the transverse ones. However, for disturbances that generate enough stretch to cause the transverse velocities to become significant the motion will instead be nonlinear. When the stretch is $\lambda < 1$, the transverse velocity becomes imaginary, the equations of motion are no longer hyperbolic, and results obtained from any scheme based on the method of characteristics would no longer be valid. Thus, we have based our scheme on the second-order equations of Eqs. (18) and (19), which are valid for all values of stretch.

Although one can argue that it is physically unrealistic to use Hooke's law for large values of stretch, we have done so to avoid the shock formations that are sure to occur with nonlinear models like the Mooney–Rivlin relation.[25] A nonlinear model would require a shock-capturing approach similar to those found in compressible fluid dynamics. Once these equations are no longer hyperbolic, their transverse velocities become imaginary, and their solutions cease to be wave-like. Thus, we hope to establish a correlation between the

nonlinear behavior of our cable and the loss of hyperbolicity that occurs when $\lambda < 1$, without the added uncertainty that would surely be introduced by a numerical shock treatment.

For a cable of unit length $l = 1$ and a uniform grid spacing of $\Delta S = 2 \times 10^{-3}$, a time-step size of $\Delta t = 5 \times 10^{-4}$ was chosen to time advance our calculations. This time-step size, based on the longitudinal wave speed, corresponds to a Courant number of 0.25 and therefore requires 2000 time steps to convect a disturbance from one end of the cable to the other (both ends fixed in space at all times). This Courant number was chosen not for numerical stability but to maintain temporal accuracy. To generate the large initial displacement that we want, we have imposed a transient pressure loading onto our cable of the form

$$\tilde{p} = |\tilde{p}|\{H[S - (0.5 - k\Delta S)] - H[S - (0.5 + k\Delta S)]\} \times \{1 - H[t - (n\Delta t)]\} \tag{29}$$

where $|\tilde{p}| = 3000$ is the magnitude of the nondimensional pressure loading, H is the Heaviside step function, $k = 4$, and $n = 10$. Thus a "top-hat" pressure distribution, nine mesh cells long and centered on the middle of the cable, is applied for 10 time steps before it is instantaneously removed. This loading adds enough energy into the system to displace the middle of the cable a distance of approximately $r_2 = 0.15$ before it is released and the cable is allowed to vibrate.

Once the pressure loading is removed, a series of disturbances are generated in opposite directions along the cable and travel toward the fixed endpoints. These disturbances reflect off the end points and travel back and forth across the cable, interacting as they pass each other at the center of the cable. Finally, after numerous reflections these disturbances are slowly damped to a steady state by the presence of the visco-elastic model.

This nonlinear wave propagation can be seen in the time sequence shown in Figs. 2–6. In each of these plots, four instantaneous cable positions are shown immediately before and after the reflected waves interact at the center of the cable. Figures 2–6 show the first wave reflections, the first interaction of the first reflected waves, the second wave reflections, the interaction of the second wave reflections, and finally the 50th wave interaction, respectively. In each case the symmetry of these results illustrates a significant lack of dispersion error, the foundation upon which our scheme was designed. In fact symmetry is maintained well beyond these 50 interactions, which, by itself, is a significant achievement because they occur 100,000 time steps beyond the initial loading and well beyond the time one might expected a numerical asymmetry to have

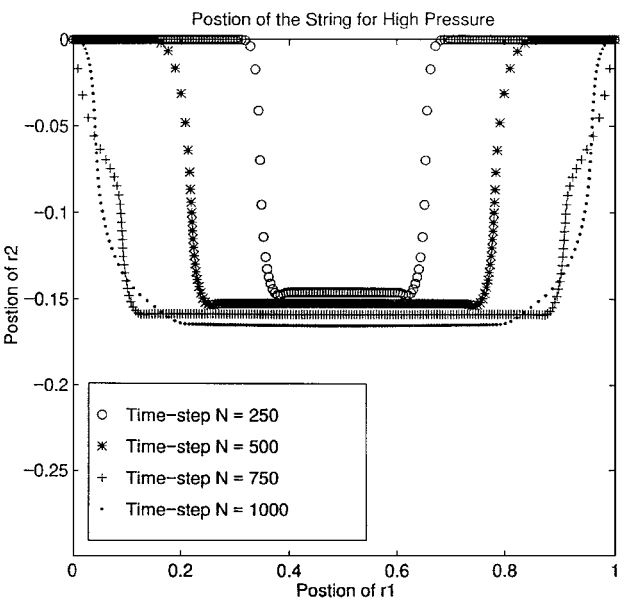

Fig. 2 String position: linearly elastic cable: first wave reflection.

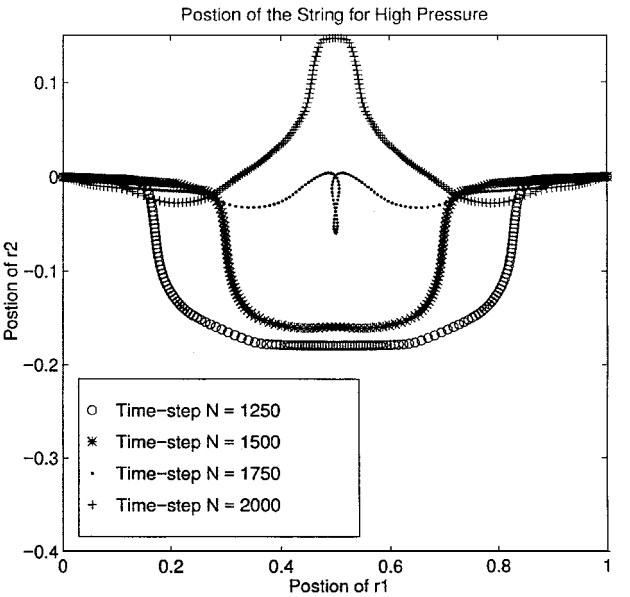

Fig. 3 String position: linearly elastic cable: first wave interaction.

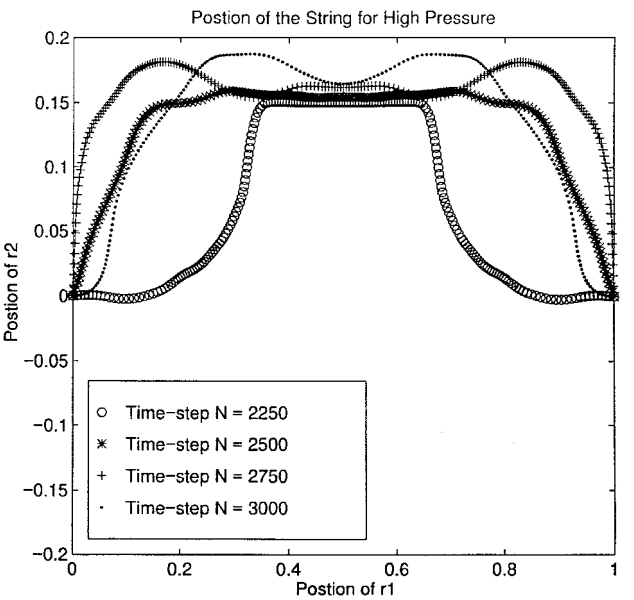

Fig. 4 String position: linearly elastic cable: second wave reflection.

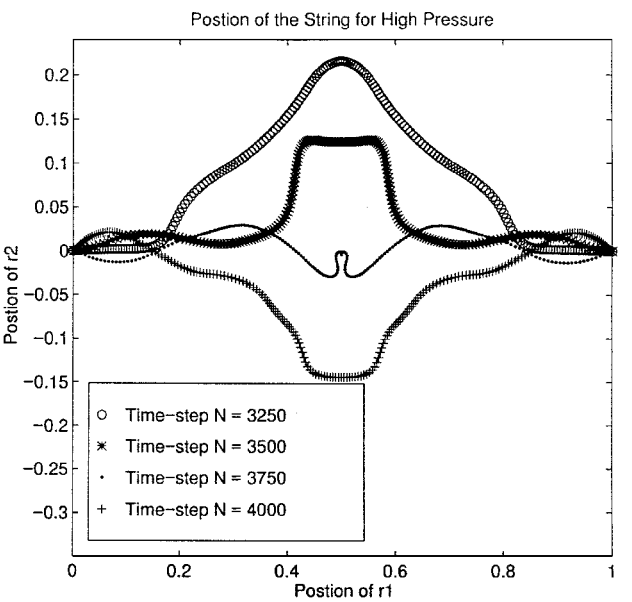

Fig. 5 String position: linearly elastic cable: second wave interaction.

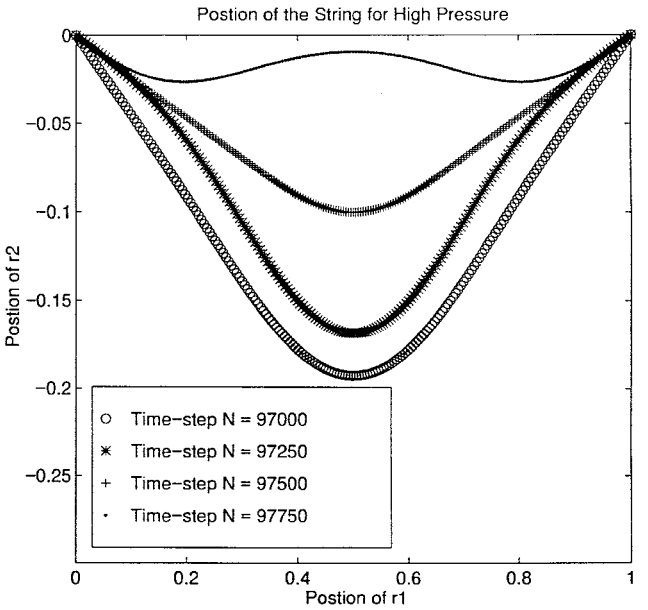

Fig. 6 String position: linearly elastic cable: 50th wave interaction.

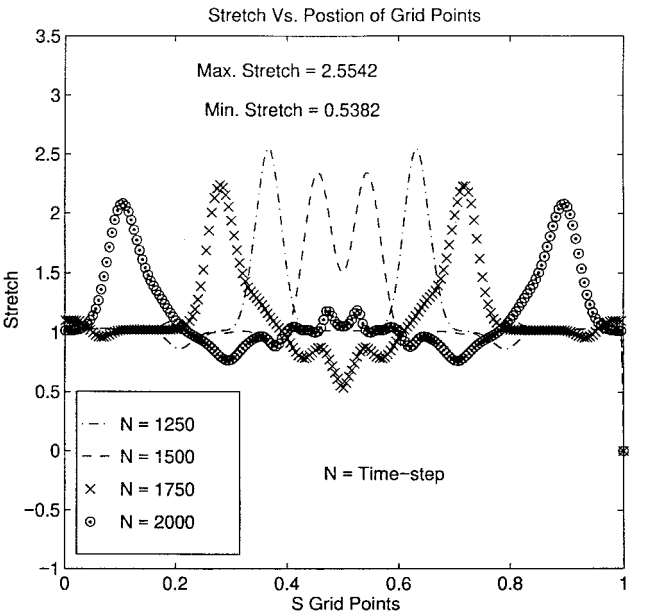

Fig. 8 Stretch: linearly elastic cable: first wave interaction.

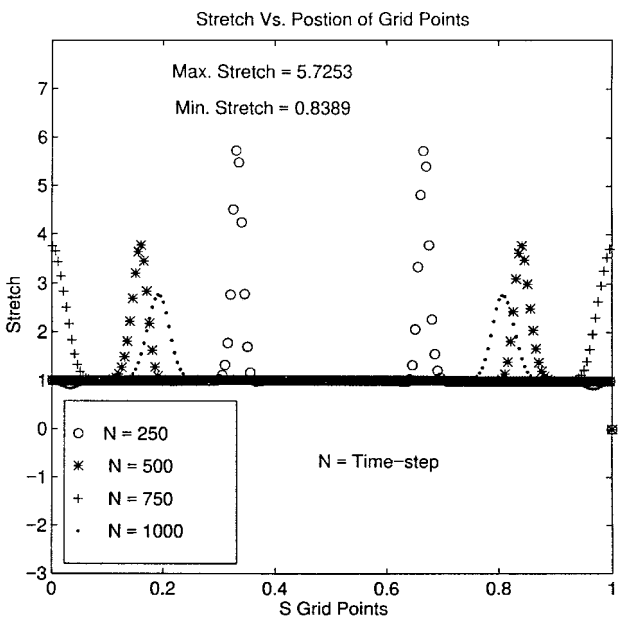

Fig. 7 Stretch: linearly elastic cable: first wave reflection.

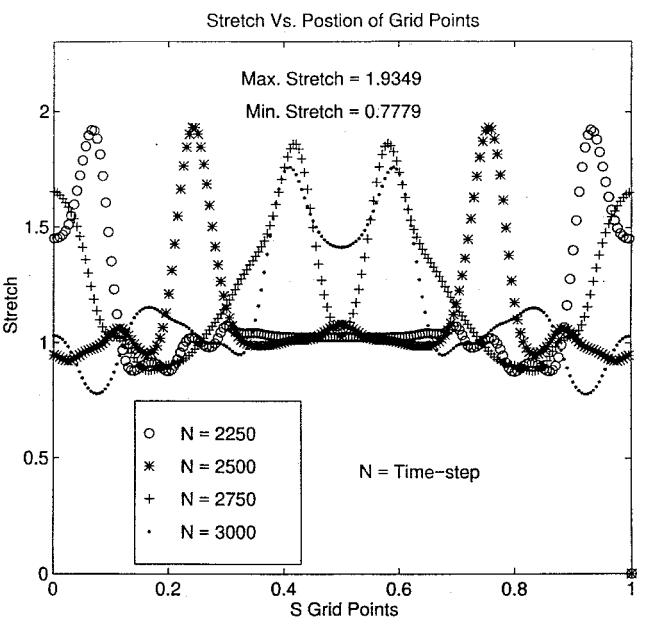

Fig. 9 Stretch: linearly elastic cable: second wave reflection.

developed. Clearly the dispersion errors within these results are minimal.

In each of these sequences, reflected waves are propagating back and forth along cable and colliding and interacting in a nonlinear fashion. Even the long duration results after 50 collisions (Fig. 6), although relatively smooth, are still significantly nonlinear. In fact the multiple inflection points that can be seen along the cable at the various moments in time are simply never created in similar small disturbance simulations.

During the first interaction, Fig. 3, we can observe a looping of the cable that is absent from the interactions at later times. In fact, a similar but significantly smaller loop was also observed during the second interaction, Fig. 5, but then never seen again.

In Figs. 7–11 we have plotted the instantaneous stretch at four moments in time immediately before and after the wave interactions that occur at the center of the cable. These results compliment the cable positions shown in Figs. 2–6 and again illustrate the symmetry of our calculations. In this sequence of results, Figs. 7–11, we find significant regions of local compression, $\lambda < 1.0$, and a general reduction in the magnitude of the stretch over time. From our simulations we have observed that these loops occur when the reflected waves interact in the center of the cable, the transverse velocity is complex, and its magnitude is roughly greater than or equal to that of its longitudinal counterpart, occurring when $\lambda < 0.5$.

Finally, we note that as this simulation was time advanced the energy added to the system by the initial pressure loading was systematically reduced by the viscous damping. In fact the time history of the total energy

$$E_T = \int_0^1 \left\{ \frac{\lambda^2}{2} - \lambda + \frac{1}{2} + \frac{1}{2}\left|\frac{\partial r}{\partial t}\right|^2 \right\} \mathrm{d}S \tag{30}$$

was damped, exponentially to zero, as the cable slowly converged to its steady state. Furthermore, no oscillations in the total energy were produced by the looping of the cable, and we note that the complexity and frequency of this looping was highly dependent on the visco-elasticity of the cable. As one might have expected, loops were more topologically complex and observed more often when the

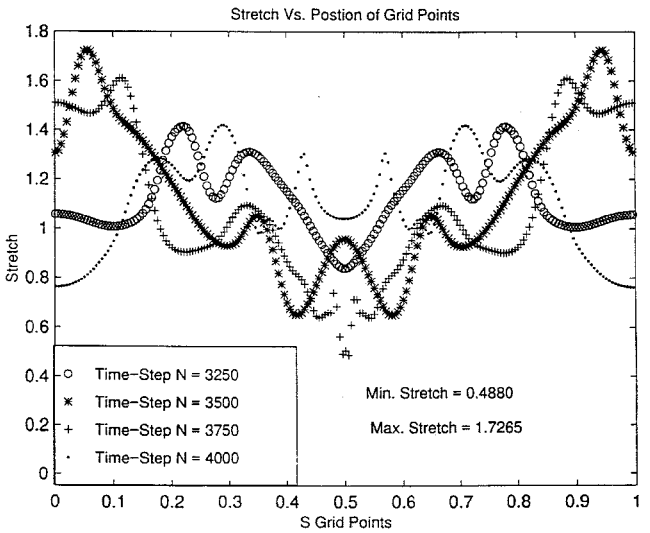

Fig. 10 Stretch: linearly elastic cable: second wave interaction.

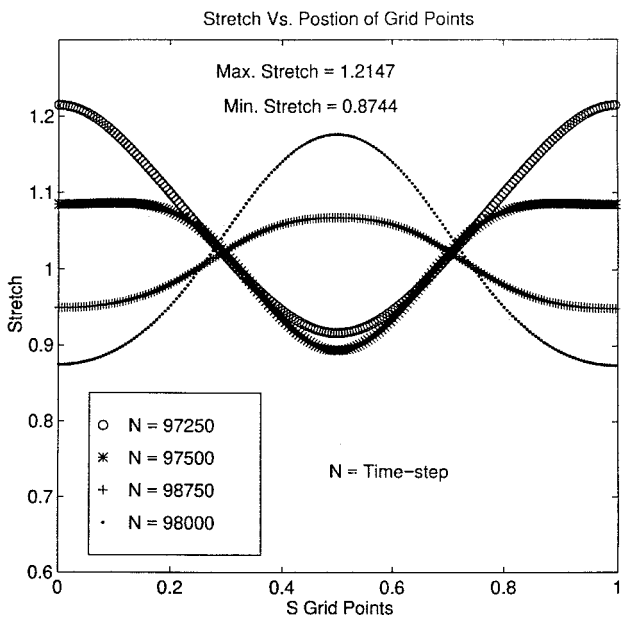

Fig. 11 Stretch: linearly elastic cable: 50th wave interaction.

cable's loss coefficient was made smaller, rather than larger. In fact, calculations run without any viscosity, often produced solutions with multiply lobed loops that did not diverge nor converge to a steady state.

VI. Conclusions

With this work we present a new technique for simulating the time-dependent behavior of an elastic material in general and the nonlinear dynamics of a linearly elastic cable in particular.

This numerical scheme approximates the system of second-order equations that governs the force balance across an elemental segment of a flexible cable. These equations were solved by a third-order-accurate, fully implicit, time integration, whose spatial terms were constructed from a second-order-accurate force balance across each of the finite mesh cells. Considerable effort was expended to tailor this numerical scheme into a form whose truncation error was both higher-order accurate and dissipative; thus, allowing us to simulate the nonlinear dynamics of an elastic material without having to account for the loss of hyperbolicity that occurs within its first-order counterpart. Furthermore, the symmetry of this spatial approximation allowed us to capture physical symmetries for durations longer than could be expected from an upwind scheme. In fact, results showed that the unloading of a visco-elastic cable could be simulated to its final equilibrium state without a loss of symmetry.

Results were presented for both the small displacement of a highly nonlinearly elastic material and the large displacement of a linearly elastic cable. The first simulation, a small displacement of a nonlinearly elastic material, was used to validate our numerical scheme against a known analytical solution, whereas the second simulation, the large displacement of a linearly elastic cable, was used to investigate the looping that can occur when wave interactions produce regions of strong local compression. This highly nonlinear motion, generated by the large displacement of the elastic material, was initiated by an impact pressure loading and unloading of a visco-elastic cable. From these simulations it was observed that loops occurred when the reflected waves interacted in the center of the cable, the transverse velocities were complex, and their magnitudes were greater than or equal to that of their longitudinal counterparts. Finally, it was also observed that the topological complexity of these loops, and the frequency of their occurrence, were highly dependent on the visco-elasticity of the cable material.

Acknowledgment

We are grateful to the Natural Sciences and Engineering Research Council of Canada for supporting this work under NSERC Grant OGP 170377.

References

[1]Kane, T. R., and Levinson, D. A., "Deployment of a Cable-Supported Payload from an Orbiting Spacecraft," *Journal of Spacecraft and Rockets*, Vol. 14, No. 7, 1977, pp. 409–413.

[2]Chen, J. C., "Response of Large Space Structures with Stiffness Control," *Journal of Spacecraft and Rockets*, Vol. 21, No. 5, 1984, pp. 463–467.

[3]Van der Ha, J. C., "Orbital and Relative Motion of a Tethered Satellite System," *Acta Astronautica*, Vol. 12, No. 4, 1985, pp. 207–211.

[4]Nowinski, J. L., "Transverse Perpendicular Impact on a Cable of Highly Elastic Material," *AIAA Journal*, Vol. 5, No. 2, 1967, pp. 332, 333.

[5]Beatty, M. F., and Haddow, J. D., "Transverse Impact of a Hyperelastic Stretched String," *Journal of Applied Mechanics*, Vol. 52, No. 1, 1985, pp. 137–143.

[6]Behbahani-Nejad, M., and Perkins, N., "Freely Propagating Waves in Elastic Cables," *Journal of Sound and Vibration*, Vol. 196, No. 2, 1996, pp. 189–202.

[7]Tait, R. J., Abdella, K., and Duncan, D. B., "Approximate Riemann Solvers and Waves on a Non-Linear Elastic String," *Computers in Mathematics with Applications*, Vol. 21, No. 4, 1991, pp. 77–89.

[8]Wegner, J. L., Haddow, J. B., and Tait, R. J., "Unloading Waves in a Plucked Hyperelastic String," *Journal of Applied Mechanics*, Vol. 56, No. 2, 1989, pp. 459–465.

[9]Shearer, M., "Nonlinear Interaction of Smoothly Travelling Waves in an Elastic String," *Wave Motion*, Vol. 7, No. 2, 1985, pp. 169–175.

[10]Antman, S. S., *Non–Linear Problems of Elasticity*, Applied Mathematics Series, Vol. 107, Springer-Verlag, New York, 1995, pp. 11–46.

[11]Antman, S. S., "Multiple Equilibrium States of NonLinearly Elastic Strings," *SIAM Journal of Applied Mathematics*, Vol. 37, No. 3, 1979, pp. 588–604.

[12]Dickey, R. W., "The Nonlinear String Under a Vertical Force," *SIAM Journal of Applied Mathematics*, Vol. 17, No.1, 1969, pp. 172–178.

[13]Eldred, L. B., Baker, W. P., and Palazotto, A. N., "Kelvin-Voigt vs Fractional Derivative Model as Constitutive Relations for Viscoelastic Materials," *AIAA Journal*, Vol. 33, No. 3, 1995, pp. 547–550.

[14]Lukasiewicz, S., and Xia, Z. Q., "Nonlinear Damped Vibrations of Simply-Supported Sandwich Plates in a Rapidly Changing Temperature Field," *Nonlinear Dynamics*, Vol. 9, No. 4, 1996, pp. 369–389.

[15]Hirch, C., *Numerical Computation of Internal and External Flows, Volume 1: Fundamentals of Numerical Discretization*, Wiley, New York, 1988, pp. 180–186.

[16]Jameson, A., "Transonic Flow Calculations for Aircraft," *Lecture Notes in Mathematics*, edited by F. Brezzi, Vol. 1127, Springer-Verlag, New York, 1985, pp. 156–242, .

[17]van Leer, B., "Towards the Ultimate Conservative Difference Scheme. II: Monotonicity and Conservation Combined in a Second-Order Scheme," *Journal of Computational Physics*, Vol. 14, No. 2, 1974, pp. 361–370.

[18]Yokota, J. W., "Diagonally Inverted Lower-Upper Factored Implicit Multigrid Scheme for the Three-Dimensional Navier-Stokes Equations," *AIAA Journal*, Vol. 28, No. 9, 1990, pp. 1642–1649.

[19]Shuen, J. S., and Yoon, S., "A Numerical Study of Chemically Reacting Flows Using a Lower-Upper Symmetric Successive Over Relaxation Scheme," *AIAA Journal*, Vol. 27, No. 12, 1989, pp. 1752–1760.

[20]Pulliam, T. H., and Chaussee, D. S., "A Diagonal Form of an Implicit Approximate Factorization Algorithm," *Journal of Computational Physics*, Vol. 39, No. 2, 1981, pp. 347–363.

[21]Jameson, A., "Time Dependent Calculations Using Multigrid, with Applications to Unsteady Flows Past Airfoils, Wings, and Helicopter Rotors," AIAA Paper 91-1596, June 1991.

[22]Jameson, A., Schmidt, W., and Turkel, E., "Numerical Solutions of the Euler Equations by Finite Volume Methods Using Runga–Kutta Time-Stepping Schemes," AIAA Paper 81-1259, June 1981.

[23]Ogden, R. W., "Large Deformation Isotropic Elasticity," *Proceedings of the Royal Society of London, Series A*, Vol. 326, No. 1567, 1972, pp. 565–584.

[24]Ogden, R. W., "Inequalities Associated with the Inversion of Elastic Stress-Deformation Relations and Their Implications," *Proceedings of the Cambridge Philosophical Society*, Vol. 81, 1977, pp. 313–324.

[25]Marsden, J. E., and Hughes, T. J. R., *Mathematical Foundations of Elasticity*, Dover, New York, 1983, p. 11.

A. N. Palazotto
Associate Editor